

Integration of Orbital and Ground Images for Enhanced Topographic Mapping in Mars Landed Missions

Ron Li, Kaichang Di, Juwon Hwangbo, Yunhang Chen
Mapping and GIS Laboratory, CEEGS, The Ohio State University
470 Hitchcock Hall, 2070 Neil Avenue, Columbus, OH 43210-1275
Tel: 614-292-4303; E-mail: {li.282, di.2, hwangbo.2, chen.1256}@osu.edu

Abstract – To date, orbital and ground image data have been mostly separately processed for topographic mapping in Mars landed missions. We are in the process of developing a method for the integration of orbital and ground image networks to enhance precision mapping. In this research, HiRISE stereo images were used as orbital data while ground data include MER-B Pancam stereo images and their pointing information. The process of estimating unknown exterior orientation parameters for the HiRISE images is explained. For orbital image processing, a semi-automatic hierarchical stereo matching technique based on image pyramid is introduced. A bundle adjustment of HiRISE stereo pair is performed. Incremental bundle adjustment technology is employed to process MER ground images, to construct a ground image network and to improve rover localization accuracy. Also, digital terrain models (DTMs) and orthophotos of Victoria Crater have been generated from the HiRISE stereo pair and are compared with those derived from the networked ground imagery.

I. INTRODUCTION

Up to now, orbital and ground image data have been mostly processed separately for topographic mapping in Mars missions. The locations of landers in the Gusev Crater and on the Meridiani Planum of the 2003 Mars Exploration Rover (MER) mission were identified by cartographic triangulation of landmarks visible in both orbital and ground images [1]. Except for such special occasions, however, orbital and ground images have been processed separately in the MER mission as well as in previous missions such as the Mars Pathfinder mission.

The development of a new technology to process orbital and ground data in a coordinated manner could provide an efficient means to resolve the frequent conflicts and inconsistencies in sensor locations, image scales, and object correspondences inherent in these two data sources.

Orbital imagers have provided global topographic information for defining the global coordinate system, for landing-site selection, and for landing site mapping. Data obtained from the Mariner 9 and Viking orbiters were used to establish the first Mars control network, which is basically a global image mosaic. Mars Global Surveyor enabled the next generation of Mars topographic surveying [2]. Its Mars Orbiter Laser Altimeter (MOLA) data was applied as a control network to reference the Mars Digital Image Mosaic (MDIM) 2.1, as well as the Mars Orbiter Camera (MOC) topographic mapping products [3, 4]. Also, topography and slope maps were produced at resolutions from 3 to 10 meters

from MOC NA (Narrow Angle) stereo images for Mars Exploration Rover (MER) 2003 mission landing-site selection [5, 6].

Ground imagers provide data at a higher level of detail, thus enabling the generation of high-precision maps of landing sites. In the MER mission, a ground image network has been built by linking all the lander and rover images with automatically and manually selected tie points. Incremental bundle adjustment was applied to the image network in order to improve accuracy of the position and orientation of the images as well as the ground location of feature points. As a result, DTMs and orthophotos of the landing sites were generated using a set of automated techniques [7].

Until the recent launch of Mars Reconnaissance Orbiter (MRO), the highest resolution orbital imagery achieved was 1.5 meters from MOC NA, while that of MER ground imagery is usually several centimeters. With the advent of the High Resolution Imaging Science Experiment (HiRISE) onboard the MRO, we are now provided with orbital imagery at a much higher resolution of 30 cm. With greatly reduced discrepancies in image scale, it is now much easier to identify common objects in both HiRISE and MER ground images. These common objects, by providing good linkage between orbital and ground image networks, enable efficient integration of these two types of Mars data.

With the support of NASA Applied Information System Research (AISR) Program, we are developing a method for the integration of orbital and ground images for enhanced topographic mapping. In this ongoing research, a combined bundle adjustment of orbital and ground imagery is used to achieve the best possible accuracy for topographic mapping. Object recognition and selection using coordinated orbital and ground image data can be enhanced to support such planetary exploration tasks such as pre-landing target selection, high-precision lander localization, and onboard navigation for the rovers.

In the reported preliminary research, the study area is Victoria Crater at the MER-B (Opportunity) landing site. The orbital data used are HiRISE stereo imagery covering the entire crater area. Due to the lack of accurate pointing information (before the official PDS release), exterior orientation (EO) parameters had to be estimated for these HiRISE images. The ground data used are Pancam stereo pairs taken by the MER-B rover around the rim of Victoria

Crater. Also, ground image networks are adopted from the existing MER operations.

We present the recent results of a hierarchical stereo-matching technique and a bundle adjustment method for the orbital images which are being developed at OSU. The bundle adjustment without ground control points is conducted for the HiRISE images. Consequently, digital terrain models (DTMs) of Victoria Crater are generated from the HiRISE stereo pair and compared with those derived from networked ground imagery.

II. DATA

In this preliminary research, HiRISE stereo images were used as orbital data while ground data include MER-B Pancam stereo pairs and their pointing information. Unknown EO parameters for the HiRISE images are estimated.

A. Orbital Data

HiRISE provides unprecedented high-resolution images with a 1.2 km-wide swath for color composites and a 6 km-wide swath for the red band. HiRISE stereo images are usually taken 17 days apart, and are obtained by re-imaging the same area from a previous orbit [8]. The first HiRISE image for Victoria Crater used in this paper, TRA_000873_1780 (0.267 m/pixel), was obtained on October 3, 2006. This image was centered at 2.1°S latitude, 5.5°W longitude. The image has a close to nadir look and all three bands (R, G, B) contain the crater. The second image, PSP_001414_1780 (0.265 m/pixel), was taken on November 14, 2006. At this point, the orbit was 90 km offset to the east and only the red band covered the entire crater.

The raw HiRISE stereo pair and the precise time index required for the derivation of EO parameters from the SPICE kernels have not yet been released to the public. But the HiRISE team released two images covering Victoria Crater, TRA_000873 image in its original format and PSP_001414 image as a map-projected version. They cannot be used for stereo processing. However, there is a released anaglyph image of Victoria Crater that combined two red-band layers of the two images covering the crater.

Since the two layers in the anaglyph are rescaled, recovering the original dimensions is necessary to “reconstruct” the images. For that purpose, the left layer was compared to its raw image (TRA_000873) to retrieve the scale factor. Victoria Crater’s size as derived from MOC NA was also used in the determination of the scale factor. The rescaled stereo images from the anaglyph were then used for testing the methods developed in this project. It should be noted that for the left image, the raw image (TRA_000873) could be used. Furthermore, the HiRISE camera calibration result has not been published and in this paper a nominal setting of the HiRISE camera using the published technical specifications is used for computation. The method and results can be improved once such information will be available.

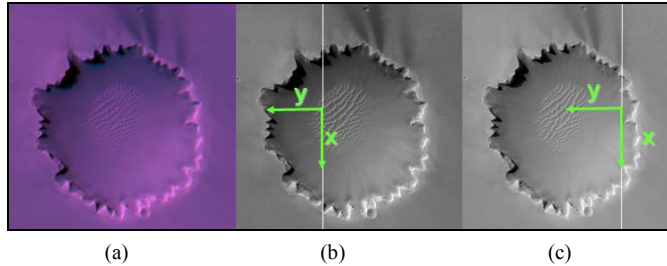


Fig. 1. Victoria Crater: (a) anaglyph, (b) rescaled left anaglyph layer, and (c) rescaled right anaglyph layer.

To determine the image coordinate system on each CCD line, its origin on the line must be identified because the image is a rescaled image. The origin on the raw image (TRA_000873) was transferred using identifiable features. The origin of each line on the right image was determined in a similar way using the projected image (PSP_001414). In Fig. 1, the white lines in the two anaglyph layers indicate the origins of the image coordinate system on each line, which are essential for 3D ground triangulation.

Orbital and ancillary data of the images can be retrieved from the SPICE kernels using the starting and ending times of image acquisition as indices. It is known with the image release that TRA_000873 was taken at 3:28 p.m. local Mars time, or 12:44 p.m. universal time. PSP_001414 was obtained 42 days later at 15:39 p.m. universal time. The time information given is not sufficient to estimate the precise orbital information from SPICE kernels. There might be an issue with a reported jitter problem [9] that may affect orientation information of the image lines.

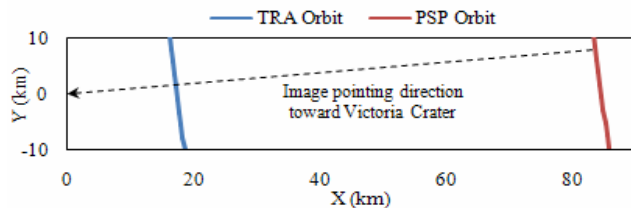


Fig. 2. MRO orbit footprint and pointing direction.

Fig. 2 shows the footprints of the MRO orbits at the approximate time indices. The issue is to find the correspondence between the two images (indexed by line IDs) and the orientation information (indexed by time). Once we find the intersection between the two orbital projects on the ground, we obtain the time for the image line containing that point, and thus we can associate time to the rest of the image. The other way to estimate the association is to use the normal space craft speed. Consequently, the time period for TRA_000873 is estimated as 12:44:16.33-64 pm, and that for PSP_001414 as 15:39:59.10-41 pm. The detailed orientation of each image lines are finally adjusted by a bundle adjustment.

B. Ground Data

The Opportunity rover has been traveling along the north

part of the Victoria Crater rim. Opportunity hard (fixed)-baseline stereo Pancam images taken on Sol 953 were used for mapping the Duck Bay area. Pancam has two frame cameras (1024×1024 pixels) of 0.27 mrad/pixel resolution with a 30-cm baseline. The position information for the rover is provided by on-board rover localization using wheel odometry, IMU, and a Sun positioning technique using Pancam imagery. Camera rotation around the mast (azimuth) and the camera bar (tilt) are recorded and serve as the initial orientation parameters.

III. ORBITAL IMAGE NETWORK

A. Stereo Matching and Tie-Point Selection

In this section, a hierarchical stereo matching technique based on an image pyramid is introduced. In addition, a bundle adjustment (BA) is conducted using tie points selected from the HiRISE stereo pair to adjust the position and orientation of each scan line.

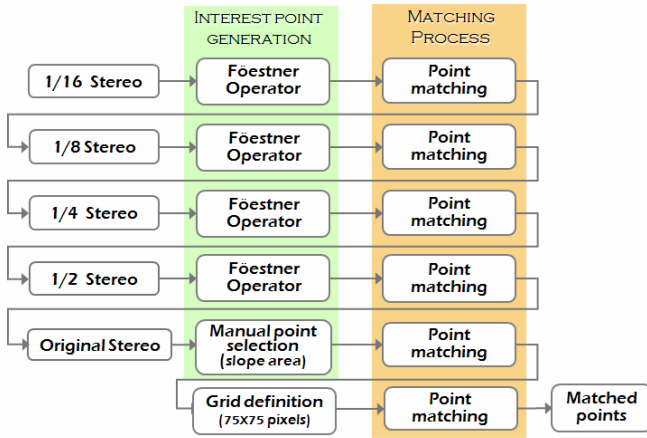


Fig. 3. Flowchart of HiRISE stereo matching procedure.

A semi-automatic hierarchical matching method was used to generate tie points from the HiRISE stereo pair. This method is based on an image pyramid with five levels: the 1/16th, 1/8th, 1/4th, 1/2nd and original level (size) of the stereo images. The matching process starts at the 1/16th level and proceeds to the original level (Fig. 3).

At the 1/16th level, interest points are automatically generated using a Förstner operator [10, 11, 12]. Interest points are matched in the stereo images using cross correlation. Points whose maximum correlation exceeds the threshold (e.g., 0.8) are selected as matched points.

Next, the locations of these matched points are adjusted to achieve maximum correlation in the 1/8th through the 1/2nd levels. New interest points are also generated by a Förstner operator and matched on the subsequent level. The search window used to match these new interest points is determined based on the parallax surface of the Delaunay triangles formed by the previously matched tie points.

At the original image level, tie points are manually selected for areas of the crater wall where interest points are often

unobtainable because the pixel brightness values are homogeneous. These manually selected points are then refined by cross correlation-based matching. In the final step, a grid with a spacing of 75 pixels is defined and corresponding points of the grid points are found by a matching process for DTM generation.

Up to the 1/2nd level, 5180 points were obtained. These were concentrated at the crater rim and the crater bottom. For the areas of crater wall, 322 points were selected manually. Finally, 2064 new points were selected from the original-size stereo images, resulting in a total of 7566 points. All of these points were used to generate the HiRISE DTM.

Sixty-six evenly distributed tie points and 221 check points were selected from the 7566 points for the subsequent bundle adjustment.

B. Bundle Adjustment for HiRISE

From the estimated time indices of the image start and end lines, EO parameters (camera positions and pointing angles) were retrieved from SPICE kernels for each image scan line. Object space coordinates of the tie points were obtained through spatial intersection. These coordinates were then projected back to the orbital images. In ideal cases, the back-projected location of a tie point should be the same as its original image location. However, imperfections in the estimated camera position and orientation can cause differences (residuals) between the original and the back-projected image coordinates. The smaller the residual, the better the EO parameters. Since there is no absolute ground control used in this bundle adjustment, the quality of the results of the bundle adjustment will be assessed based on these residuals.

Since the orbital image was acquired within a short period of time, we can assume that the EO parameters only change linearly, along the image scan lines. The positions and pointing angles of the HiRISE sensor can be parameterized with first-order polynomial (i.e., linear) models. In this case, the model can be described as

$$\begin{aligned} X_S^i &= a_0 + a_1 i & Y_S^i &= b_0 + b_1 i & Z_S^i &= c_0 + c_1 i \\ \omega_S^i &= d_0 + d_1 i & \phi_S^i &= e_0 + e_1 i & \kappa_S^i &= f_0 + f_1 i \end{aligned} \quad (1)$$

where X_S^i , Y_S^i , and Z_S^i represent the camera position on the i^{th} row (scan line); ω_S^i , ϕ_S^i , κ_S^i are the camera pointing angles on that row; and a_0 , a_1 , ..., f_0 and f_1 are the coefficients of the linear model [14]. In the bundle adjustment, the initial values for the polynomial coefficients were estimated by fitting the original exterior orientation data retrieved from the SPICE kernels. Solving for these 12 coefficients, instead of the actual EO parameters of each scan line, ensures that results of this bundle adjustment processing are more stable and accurate.

IV. GROUND IMAGE NETWORKS

A ground image network is constructed by linking with tie points the panoramas and images taken along the rover

traverse. Intra-stereo tie points link the left and right images of a Pancam or a Navcam stereo pair. Inter-stereo tie points link adjacent stereo pairs within one panorama. Cross-site tie points link images from adjacent panoramas acquired at rover sites that are usually tens of meters apart. Bundle adjustment of this image network provides accurate image orientation parameters and ground positions of tie points. Consequently, high-precision rover localization and topographic mapping can be achieved [1].

A. Ground Image Tie-Point Selection

Intra-stereo tie points link the left and right images of one stereo pair. Förstner interest points [10] are extracted as features from these images and then matched using cross correlation matching and least-squares matching applied with constraints such as epipolar and bi-directional uniqueness [15]. To verify the match, parallaxes of matched interest points are examined to eliminate extreme outliers from parallax curve. Since an unstructured natural terrain is generally piece-wise continuous, parallax decreases generally from top to bottom. Spatial intersection is conducted to derive

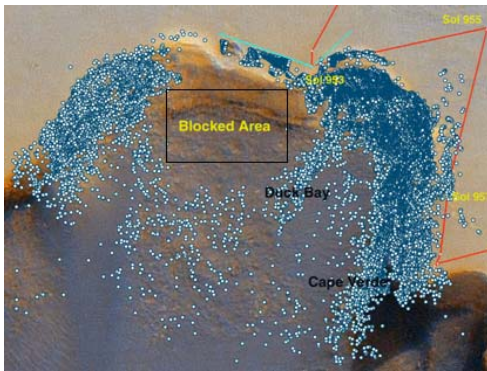


Fig. 4. Distribution of 3D tie points at Duck Bay.

coordinates in 3D object space for these tie points. Fig. 4 shows the 3D location of tie points acquired from 26 pairs of Pancam stereo images of Duck Bay in Victoria Crater. These ground points were later used to generate a ground DTM (see Fig. 9) of Duck Bay after bundle adjustment.

Inter-stereo registration is generally more difficult than intra-stereo registration since the ratio of overlap between inter-stereo images is only around 10% instead of more than 90% for intra-stereo images. A matched intra-stereo tie point from one stereo pair is first projected to the adjacent stereo pair using a triangulated 3D ground position and the original EO parameters. Then, cross correlation matching and least-squares matching are conducted by searching in a very small area. After parallax verification, matched interest points can be used as inter-stereo tie points. Usually too many matched interest points that could serve as intra- and inter- stereo tie points are found. A gridding strategy is employed to limit this number of tie points by picking the most reliable tie point in each grid cell [15].

Cross-site tie points are even more difficult to find due to the significant differences between different panoramas in image resolutions, looking angles, and illumination conditions. Recently, we developed an innovative method for automatic cross-site tie-point selection based on modeling and matching of rocks from adjacent rover sites [16]. Rocks are extracted from dense 3D ground points generated by stereo matching, and then modeled using such analytical surfaces as hemispheroids, semi-ellipsoids, cones and tetrahedrons. Modeled rocks are matched from two rover sites by a combination of rock-modeling matching and rock-distribution-pattern matching. The resulting matched rocks are used as cross-site tie points for the bundle adjustment [17].

B. Bundle Adjustment of the Ground Image Network

Bundle adjustment of the ground image network minimizes any inconsistencies between the image EO parameters and the 3D positions of the tie points [17]. Although bundle adjustment of MER data is basically identical to that for any frame camera, there are certain constraints, which can be incorporated into the observation equations to make the adjustment computation more accurate and reliable [18]. The relative orientation and distance between the left and right stereo cameras are fixed, and all the Pancam and Navcam stereo cameras have the same distance to the rotation axis. During MER mission operations, bundle adjustment of the image network has usually improved 3D accuracy from tens of pixels to a sub-pixel to 1 pixel level. It has improved 3D accuracy from a meter to a centimeter level within a local area [1].

V. RESULTS

A. Orbital Image Bundle Adjustment

The bundle adjustment of the orbital image data requires good estimations of the initial values for its unknowns. Since the exact image acquisition times are not yet available to us, we estimated their start times such that the back-projection residuals were minimal (2 pixels on average). Through bundle adjustment, the camera positions and pointing angles were adjusted based on the linear model. Sixty-six tie points were used in the bundle adjustment and 221 independent check points were used to evaluate the accuracy of the BA. After BA, the back-projection residuals for the check points were reduced, on average, from 2.0 to 0.7 pixels.

Values of the coefficients in (1) after BA are used to calculate the six EO parameters for each scan line. Changes in camera positions were, on average: 26 cm for Z_S^i , and less than 5 cm for X_S^i and Y_S^i . Changes in pointing angles (ω_S^i , φ_S^i , and κ_S^i) were less than five seconds.

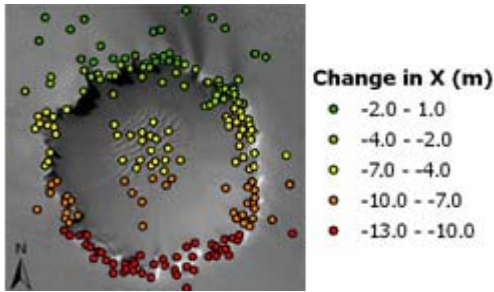


Fig. 5. Changes in ground coordinates after BA.

After BA, the 3D ground coordinates of the tie points are derived from triangulation (space intersection) using the adjusted camera position and pointing data. Fig. 5 demonstrates the amount of change in the X component of ground coordinates in the Mars body fixed coordinate system after bundle adjustment. The Y and Z components change very little (less than 1 meter). Point positions in the northern part change very little, while points in the southern part have corrections larger than 10 meters. This correction matches the more significant reduction of back-projection residuals of those points on the south.

B. DTMs from HiRISE

The 3D coordinates of the 7566 matched points in object space were obtained by photogrammetric triangulation using original EO parameters without bundle adjustment. Subsequently, Kriging interpolation was performed to generate a DTM and an orthophoto of Victoria Crater (Fig. 6). This DTM has a crater diameter of 750 meters.



Fig. 6. Victoria Crater 3D view created by draping orthophoto on DTM.



Fig. 7. Victoria Crater DTMs (vertically exaggerated by a factor of 3) before (red) and after (blue) BA.

Another DTM of Victoria Crater was generated in the same way except for using bundle-adjusted EO parameters. In Fig. 7, DTMs of the original (in red) points and the bundle-adjusted (in blue) points are shown overlaid. After bundle adjustment, the southern half of the DTM moved downward,

while northern half went upward. Middle points along the east-west direction barely changed positions. Overall, the change in the original DTM caused by the bundle adjustment is a slight rotation (about 0.78°) around an axis of east-west direction.

C. HiRISE DTM Validation

To validate the HiRISE DTM generated after bundle adjustment, we compared it to the BA-based MER localization data and to a local DTM derived from ground imagery. The BA-based localization was performed locally along the rim of Victoria Crater. Six landmarks were measured from the bundle-adjusted rover images and overlaid

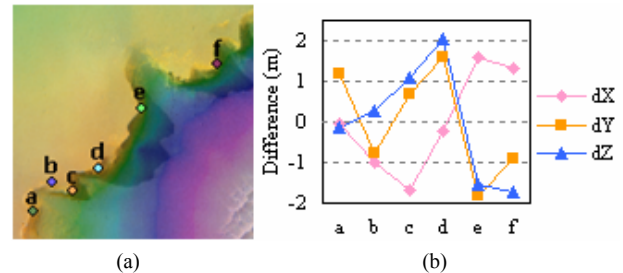


Fig. 8. (a) Six landmarks at Victoria Crater overlaid on HiRISE DTM; (b) Positional differences between HiRISE and MER DTMs.

on the HiRISE DTM (Fig. 8a). The positions of the six landmarks were defined in the local coordinate system, where the X, Y, and Z axes represent the east/west, north/south, and vertical directions, respectively. The coordinates of these landmarks from both orbital and ground localization results were compared and shifted so that the sum of the residuals in Fig. 8(b) is zero. Standard deviations of residuals in X, Y and Z are 1.28 m, 1.35 m, and 1.48 m, respectively.

The HiRISE DTM of Duck Bay was then compared to the DTM generated from the bundle-adjusted Pancam images of that area to further validate the HiRISE DTM (Fig. 9). Before comparison, both DTMs are registered horizontally by matching the ground orthophoto to the HiRISE image. Also, a vertical adjustment is made so that the difference in average elevation between the two DTMs is zero. Differences in horizontal position of six common features are measured to evaluate the horizontal difference between the two DTMs. Standard deviations of residuals in X and Y are 0.43 m and 0.75 m. Vertical differences are depicted by the differences in elevation between the two DTMs. The standard deviation of elevation difference is 1.25 m.

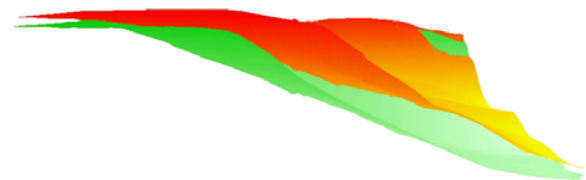


Fig. 9. Duck Bay: ground (green) and HiRISE (red) DTMs.

VI. CONCLUSIONS

In this research, a methodology for orbital data processing was developed and examined. A semi-automatic hierarchical matching technique was developed and used to derive tie points and DTM points from HiRISE stereo pairs. The adjustment of orbital image EO parameters resulted in reduced back-projection errors. From orbital data, DTMs were generated for the Victoria Crater study site. The ground image network was constructed and adjusted using bundle adjustment. DTMs derived from HiRISE and MER stereo pairs were compared. The differences between them were less than 2 meters in any direction. Note that the HiRISE data used in this research are not the raw images that preserve the imaging geometry. The accurate EO parameters are not available due to the lack of exact image acquisition time information. We expect that when raw images with accurate EO parameters are made available, we should have improved results.

In order to integrate orbital and ground image networks, common objects must be identified from both types of images; thus our future task is to develop efficient recognition and matching procedures for finding these corresponding objects. Inconsistencies in resolution and viewing angle are major challenges to the integration of these two types of data. To resolve these issues, we will use as matching criteria those 3D coordinates of the terrain that have been generated in our previous work. Totally integrated image networks would include a coordinated bundle adjustment of both types of data. Also, fully automated matching would be beneficial for processing homogeneous regions such as the areas of crater wall.

ACKNOWLEDGMENT

We would like to acknowledge support from the NASA Applied Information System Research (AISR) program.

REFERENCES

- [1] Li, R., et al., "Initial results of rover localization and topographic mapping for the 2003 mars exploration rover mission," *Photogrammetric Engineering & Remote Sensing*, Vol. 71, No. 10, 2005, pp. 1129–1142.
- [2] Shan, J., et al., "Photogrammetric analysis of the Mars Global Surveyor mapping data," *Photogrammetric Engineering & Remote Sensing*, Vol. 71, No. 1, 2005, pp. 97–108.
- [3] Archinal, B.A., et al., "A new Mars Digital Image Model (MDIM 2.1) control network," *XXth ISPRS Congress*, Istanbul, Turkey, July 2004.
- [4] Archinal, B.A., et al., "Mars Digital Image Model 2.1 control network," *Lunar and Planetary Science XXXIV*, Huston, Texas, 2003, #1485.
- [5] Anderson, F.S., and T.J. Parker, "Characterization of MER landing sites using MOC and MOLA," *Lunar and Planetary Science XXXIII*, League City, Texas, March 2002, #2028.
- [6] Golombek, M. P., et al., "Selection of the Mars Exploration Rover landing sites," *J. Geophys. Res.*, Vol. 108, E12, doi:10.1029/2003JE002035, 2003.
- [7] Li, R., K. Di, and F. Xu, "Automatic Mars landing site mapping using surface-based images," *ISPRS WG IV/9: Extraterrestrial Mapping Workshop on Advances in Planetary Mapping*, Houston, Texas, 2003.
- [8] Smrekar, S.E., et al., "Mars Reconnaissance Orbiter's first look at mars," *Lunar and Planetary Science XXXVIII*, 2007, #2126.
- [9] Kirk, R.L. et al., "Ultrahigh resolution topographic mapping of mars with HiRISE stereo images: methods and first results," *Lunar and Planetary Science XXXVIII*, 2007, #1428.
- [10] Förstner, W., "A feature based correspondence algorithm for image matching," *Intl. Arch. Photogrammetry Remote Sensing*, vol. 26, pp. 150–166, 1986.
- [11] Schmid, C., R. Mohr, and C. Bauckhage, "Evaluation of interest point detectors," *International Journal of Computer Vision*, vol. 37, pp. 151–172, 2000.
- [12] Zitova, B., J. Flusser, J. Kautsky, and G. Peters, "Feature point detection multiframe images," *Proceedings of the Czech Pattern Recognition Workshop*, 2000, pp. 117-122.
- [13] Yoon, J., and J. Shan, "Combined bundle adjustment of MOC stereo images and MOLA altimetry data for precise Mars topographic mapping," *XXth ISPRS Congress*, Istanbul, Turkey, July 2004.
- [14] Li, R., G. Zhou, A. Gonzalez, J.K. Liu, F. Ma, and Y. Felus, "Coastline mapping and change detection using one-meter resolution satellite imagery," *ISPRS COM.III Symp.*, Columbus, OH, July 1998.
- [15] Xu, F., "Automation in Mars Landing-Site Mapping and Rover Localization," *XXth ISPRS Congress*, Istanbul, Turkey, July 2004.
- [16] Li, R., K. Di, A. Howard, L. Matthies, J. Wang, and S. Agawal, "Rock modeling and matching for autonomous long-range Mars rover localization," *Journal of Field Robotics*, Vol. 24, No. 3, 2007, pp. 187–203.
- [17] Li, R., K. Di, L.H. Matthies, R. Arvidson, W. M. Folkner, and B.A. Archinal, "Rover Localization and Landing Site Mapping Technology for the 2003 Mars Exploration Rover Mission," *Photogrammetric Engineering & Remote Sensing*, Vol. 70, No. 1, 2003, pp. 77–90.
- [18] Di, K., F. Xu and R. Li, "Constrained Bundle Adjustment of Panoramic Images for Mars Landing Site Mapping," in *Mobile Mapping Technologies*, *ISPRS Book Series*, Tao, V. and J. Li Eds. Taylor & Francis, 2007, pp. 109-118.